


Probing Time Dilation in Coulomb Crystals in a High-Precision Ion Trap

J. Keller,* D. Kalincev, T. Burgermeister, A. P. Kulosa, A. Didier, T. Nordmann, J. Kiethe, and T.E. Mehlstäubler

Physikalisch-Technische Bundesanstalt, Bundesallee 100, 38116 Braunschweig, Germany

 (Received 24 March 2018; revised manuscript received 21 October 2018; published 7 January 2019)

Trapped-ion optical clocks are capable of achieving systematic fractional frequency uncertainties of 10^{-18} and possibly below. However, the stability of current ion clocks is fundamentally limited by the weak signal of single-ion interrogation. We present an operational, scalable platform for extending clock spectroscopy to arrays of Coulomb crystals consisting of several tens of ions while allowing systematic shifts as low as 10^{-19} . We observe three-dimensional excess micromotion amplitudes inside a Coulomb crystal with atomic spatial resolution and subnanometer amplitude uncertainties, and show that in ion Coulomb crystals of length $400\ \mu\text{m}$ and $2\ \text{mm}$, time-dilation shifts of In^+ ions due to micromotion can be close to 1×10^{-19} and below 10^{-18} , respectively. In previous ion traps, excess micromotion would have dominated the uncertainty budget for spectroscopy of even a few ions. By minimizing its contribution and providing a means to quantify it, we open up a path to precision spectroscopy in many-body ion systems, enabling entanglement-enhanced ion clocks and providing a well-controlled, strongly coupled quantum system.

DOI: [10.1103/PhysRevApplied.11.011002](https://doi.org/10.1103/PhysRevApplied.11.011002)

I. INTRODUCTION

Optical atomic clocks [1] are currently the most accurate man-made devices, capable of providing frequency references with fractional uncertainties approaching one part in 10^{18} . The two most successful approaches thus far are ensembles of 10^3 – 10^4 neutral atoms stored in an optical lattice (e.g., Refs. [2–5]), and single trapped ions (e.g., Refs. [6–8]). The latter benefit from the ability to be strongly confined due to their charge, which, to first order, does not affect the electronic energy structure (by definition, the time-averaged electric field vanishes at the equilibrium ion position). The resulting strong localization and excellent control over the trapping environment for single ions are an ideal premise for high-accuracy spectroscopy. Besides being excellent candidates for optical clocks, ions also provide transitions with high sensitivities for tests of general relativity [9,10] or the search for physics beyond the standard model [11–13]. Stable and reproducible optical clocks also give rise to novel applications such as chronometric leveling, which uses relativistic time dilation to determine differences in gravitational potential [14,15]. With a fractional frequency resolution of 1×10^{-18} , corresponding to 1 cm of height difference on Earth's surface, optical clocks become competitive sensors for geodesy [16–18].

However, current single-ion clocks are fundamentally limited by their statistical uncertainty due to the low

signal-to-noise ratio of a single quantum absorber [19]. The corresponding instabilities on the order of $10^{-15}/\sqrt{\tau}$ necessitate measurement times τ of tens of days before the atomic transition frequency is resolved to within 10^{-18} . These long integration times complicate comparisons between clocks and significantly impede practical applications. So far, it has been unclear whether precision spectroscopy can be extended to many ions to provide fast and ultrastable clock spectroscopy [20–22] without compromising accuracy. Here we demonstrate the possibility to scale the high level of control from a single ion to spatially extended and strongly coupled many-body systems with corresponding systematic uncertainties as low as 1×10^{-19} . A clock based on N ions can reach a given instability N times faster, and further allows the implementation of novel clock schemes, such as cascaded interrogation of separate ensembles [23,24] or the use of quantum correlations [25–27]. The unperturbed storage of extended multi-ion ensembles demonstrated here is also a key requirement for scaling ion-based quantum-simulation [28–30] and quantum information processing [31] systems to sizes and computation times at which they outperform classical computations.

In this work, we present the operation of a platform for precision spectroscopy. In previous clock ion traps, micromotion-induced time-dilation shifts increased by 10^{-17} over $3\ \mu\text{m}$ [6] (or 10^{-18} over $20\ \mu\text{m}$ [32]). Our platform is capable of storing $400\text{-}\mu\text{m}$ -long ion chains with shifts close to 1×10^{-19} . This is shown with the use of a measurement technique that images time-dilation

*jonaskeller@gmx.de

shifts with 10^{-20} resolution for each individual ion within a Coulomb crystal. Since these findings resolve one of the major concerns in precision spectroscopy with ion ensembles, they are a crucial prerequisite for future clocks based on this approach. In combination with a detailed analysis of further systematic shifts [33], they allow us to show that the overall contribution of multi-ion operation to the frequency uncertainty of an In^+ clock can be below 1×10^{-19} . Our approach supports ion numbers on the order of 100 at this level of accuracy. The scalability of our ion trap platform is also useful for cascaded clock operation and storage of quantum information.

II. ION TRAP ARRAY

Our platform consists of a linear rf trap array [shown in Figs. 1(a)–1(c)] developed for precision spectroscopy on separate ion ensembles. In this type of trap, large Coulomb crystals can be stored to serve as high-stability frequency references, while short chains on the order of ten ions allow clock operation with high accuracy [see Figs. 1(d) and 1(e)]. Separation into relatively small linear crystals limits the complexity of the motional spectrum, provides approximately homogeneous environmental conditions, and supports internal state read-out with single-ion resolution, while further scaling is achieved by the storage of multiple such ensembles. The trap array consists of four AlN wafers with gold electrodes, the geometry of which is based on the calculations in Ref. [21]. Assembly

from a small number of laser-cut monolithic wafers with laser-structured gold layers ensures scalability and symmetrically shaped electrodes with manufacturing tolerances below $10 \mu\text{m}$. Integrated Pt100 sensors allow *in situ* temperature measurements during clock operation. Further trap features include three-dimensional (3D) optical access, dedicated electrodes for 3D stray-field compensation in each segment, and integrated RC filters close to each electrode to prevent pickup electronic noise from exciting eigenmodes of the Coulomb crystals. The electrical design was previously tested in a simple prototype trap [34].

III. TIME DILATION IN ION COULOMB CRYSTALS

The strongest concern for precision spectroscopy in extended ion many-body systems is the time dilation due to fast motion of individual ions, driven by the confining rf field at Ω_{rf} [excess micromotion (EMM)]. Our concept relies on the storage of all ions at positions of minimal rf-field amplitude, and is therefore not restricted to atomic species that allow cancellation of micromotion-induced ac Stark and time-dilation shifts [35]. This choice also avoids ion heating by an rf-enabled coupling of noise at frequencies of $\Omega_{\text{rf}} \pm \omega_i$ to motional modes at ω_i [36]. However, while a single ion can be placed at the point of lowest (ideally, vanishing) rf-field amplitude by the application of static electric fields (see, e.g., Refs. [37–40]), doing so with a chain of ions relies on the existence of a true

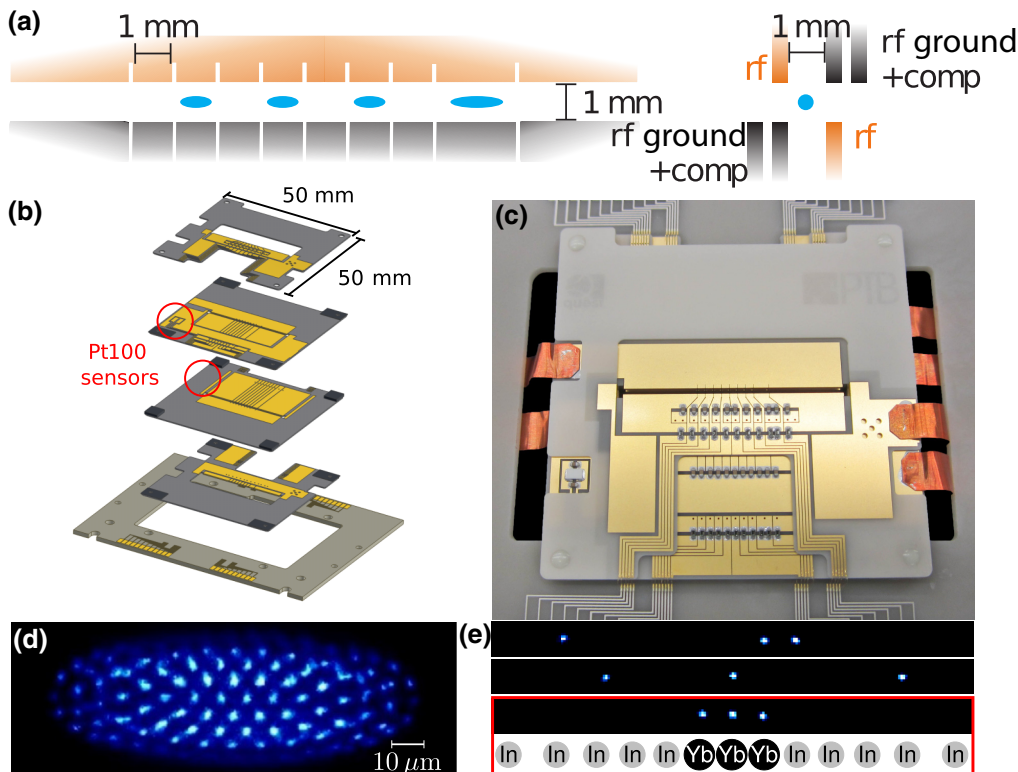
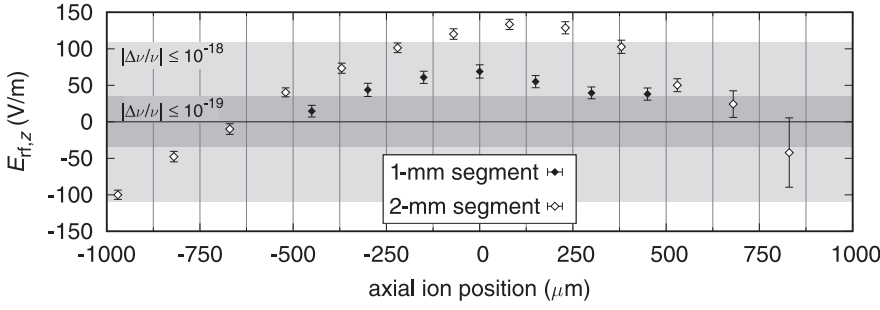


FIG. 1. Precision scalable ion-trap array. (a) Electrode geometry: the trap consists of one 2-mm-long segment and seven 1-mm-long segments, ‘comp’ refers to stray-field compensation voltages. (b) Trap assembly from a stack of four wafers. (c) Photograph of the trap, showing the onboard low-pass filters and one thermistor. (d) Large Coulomb crystal (here Yb^+ ions), which can serve as a high-stability frequency reference. (e) Linear In^+ (dark)/ Yb^+ (fluorescing) crystals. The bottom configuration is chosen for high-accuracy clock operation. Its axial length is $219 \mu\text{m}$ ($61 \mu\text{m}$) for $\nu_{\text{ax}} = 30 \text{ kHz}$ ($\nu_{\text{ax}} = 205 \text{ kHz}$), the parameters used in Ref. [33].



nodal line in the trapping field. Axial rf-field components prevent the formation of such a line when the translation symmetry of the trap is broken by its finite length, segmentation, and possible manufacturing imperfections. Secondly, the line of minimal rf amplitude is not necessarily identical to the line of minimal radial potential, and it is not clear that the available compensation fields can correct for this over the whole extent of the crystal. Finally, collective effects exist within the crystal, in which ions are affected by the fluctuating Coulomb repulsion from neighboring ions undergoing micromotion [22,41]. We show in the Supplementary Material [42] that this last effect scales as $(\omega_{ax}/\Omega_{rf})^2$ in linear ion chains at an axial trapping frequency ω_{ax} and is negligible for our parameters.

A. Single-ion time-dilation measurements

Using a photomultiplier tube (PMT) and the photon-correlation technique [43], we previously demonstrated the capability of quantifying the frequency shifts resulting from EMM with uncertainties below 10^{-20} for a single ion [38]. Here, using this technique, we first benchmark the trap array by measuring the micromotion amplitudes $z_{0,EMM}^{(Yb)}$ of a single $^{172}\text{Yb}^+$ ion at different positions along the trap axis. The observed rf-electric-field amplitudes $E_{rf,z} = m_{Yb}\Omega_{rf}^2 z_{0,EMM}^{(Yb)}/e$ are below 80 V/m (140 V/m) over an entire 1-mm-long (2-mm-long) segment, as shown in Fig. 2. The corresponding fractional time-dilation shifts for $^{115}\text{In}^+$, $|\Delta\nu/\nu_0| = (\Omega_{rf} z_{0,EMM}^{(In)})^2/(2c^2) = (\Omega_{rf} z_{0,EMM}^{(Yb)})^2/(2c^2)(m_{In}/m_{Yb})^2$, are below 5.3×10^{-19} (1.6×10^{-18}). In these relations, m_{Yb} and m_{In} denote the respective ion mass, c denotes the speed of light, and e denotes the elementary charge (see Supplemental Material at [42] for a comprehensive list of relations between measures of EMM). The change in time-dilation shift over a characteristic ion distance of $10 \mu\text{m}$ is below 4×10^{-20} everywhere in these segments, with a gradient 3 orders of magnitude smaller than previously reported [6]. The resulting axial range with shifts below 10^{-18} allows the storage of more than 50 ions in each segment.

The question remains whether single-ion measurements can predict the rf-driven motion of multiple simultaneously trapped ions. We have therefore developed a method to

FIG. 2. Single-ion measurements of the axial rf-field component in two trap segments of length 1 and 2 mm, respectively, at an rf amplitude of $U_{rf} \approx 800$ V. The shaded areas correspond to time-dilation shifts below 10^{-18} (10^{-19}) for $^{115}\text{In}^+$.

simultaneously observe EMM in individual ions within a Coulomb crystal.

B. Stroboscopic imaging technique

Our experimental setup for spatially resolved micromotion measurements in Coulomb crystals is shown in Fig. 3(a): Ion fluorescence is imaged onto an image intensifier (Proxivision BV 2581 TZ 5N), the cathode of which is driven with 10-ns square pulses, corresponding to about one quarter of the rf period. These pulses are triggered by the trap drive, with a variable delay δt to adjust the relative phase. Details on the electronic circuit can be found in Ref. [44]. Photoelectrons are subsequently multiplied by a multichannel-plate assembly and converted back to photons by acceleration onto a fluorescent screen. Finally, the screen image is observed with an electron-multiplying CCD camera and integrated separately for each of four phase settings and three laser directions. All 12 settings are interleaved, and the collected images are added up in postprocessing. Figure 3(b) shows an example of such an image with a total exposure of 2700 s. The spatial resolution is slightly deteriorated by the image intensifier, as the applied cathode pulses of approximately 100 V are half of the design value, allowing more transverse electron motion

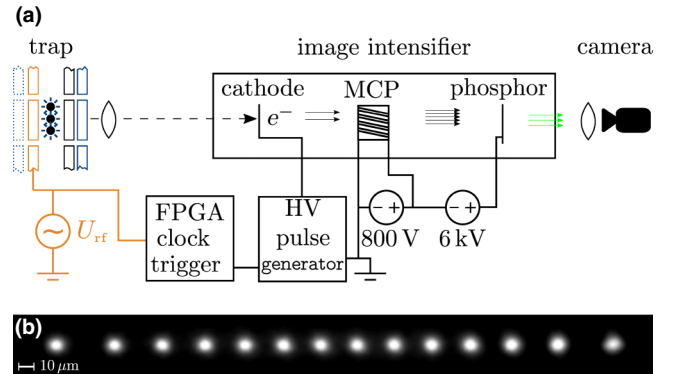


FIG. 3. (a) Setup for stroboscopic micromotion measurements across Coulomb crystals with atomic resolution. (b) Stroboscopic image of a 14-ion $^{172}\text{Yb}^+$ crystal for one rf-phase and laser direction setting with a total integration time of 2700 s. FPGA, field-programmable gate array; HV, high voltage; MCP, microchannel plate.

during the time of flight. Since the mean photon number during each gate pulse is about 4×10^{-5} per ion, mutual electron repulsion at this stage is negligible. Individual ions can be clearly resolved in the final image, and circular regions of interest are used to separate their signals. No modulation is observed in stray light imaged with this setup, ensuring that there is no additional modulation due to, for example, electronic noise at the trap drive frequency.

We use $^{172}\text{Yb}^+$ ions as probes for the rf electric field. Fluorescence from the $^2S_{1/2} \leftrightarrow ^2P_{1/2}$ transition at 370 nm is modulated by EMM as

$$S(t) = S_0 + \Delta S \cos(\Omega_{\text{rf}} t). \quad (1)$$

The transfer function of the image-intensifier setup can be written as

$$d(t) = \left[\text{rect} \left(\frac{1}{\alpha} \frac{\Omega_{\text{rf}}}{2\pi} t - \delta t \right) + \xi(t - \delta t) \right] * \text{comb} \left(\frac{\Omega_{\text{rf}}}{2\pi} t \right), \quad (2)$$

where rect and comb are the rectangular and Dirac comb functions, $\alpha < 1$ is the fraction of the rf period for which the intensifier is gated, $\xi(t)$ accounts for a possible deviation from ideal rectangular pulses, and the asterisk denotes convolution. The observed signal is the product of Eqs. (1) and (2), integrated over the detection time:

$$\begin{aligned} O &= \int_{t_{\text{det}}} S(t) d(t) dt \\ &= S_0 \int_{t_{\text{det}}} d(t) dt + \Delta S \int_{t_{\text{det}}} \cos(\Omega_{\text{rf}} t) d(t) dt \\ &= S_0 \int_{t_{\text{det}}} d(t) dt + \Delta S \int_{t_{\text{det}}} \text{Re} \left(e^{i\Omega_{\text{rf}} t} \right) d(t) dt \\ &\approx S_0 D(0) + \Delta S \text{Re} [D(\Omega_{\text{rf}})], \end{aligned} \quad (3)$$

where the last step assumes $t_{\text{det}} \gg 2\pi/\Omega_{\text{rf}}$, such that the integration limits can be replaced by $\pm\infty$, $D(\omega)$ is the Fourier transform of $d(t)$,

$$\begin{aligned} D(\omega) &\propto \left[\text{sinc} \left(\pi \alpha \frac{\omega}{\Omega_{\text{rf}}} \right) + \Xi(\omega) \right] \\ &\quad \times \text{comb} \left(\frac{\omega}{\Omega_{\text{rf}}} \right) \times e^{i\delta t/\Omega_{\text{rf}}}, \end{aligned} \quad (4)$$

and $\Xi(\omega)$ is the Fourier transform of $\xi(t)$. By adjustment of δt , the magnitude of $\text{Re}[D(\Omega_{\text{rf}})]$ is varied to distinguish the ΔS and S_0 contributions:

$$\begin{aligned} O(\delta t) &= S_0 D(0) + \Delta S |D(\Omega_{\text{rf}})| \cos(\Omega_{\text{rf}} \delta t) \\ &\propto [1 + \Xi(0)] S_0 \\ &\quad + [\text{sinc}(\pi \alpha) + \Xi(\Omega_{\text{rf}})] \Delta S \cos(\Omega_{\text{rf}} \delta t). \end{aligned} \quad (5)$$

The quantity $\Delta S/S_0$, which is used to determine the micromotion amplitude [38], is thus observed with a contrast of

$$C = \frac{\text{sinc}(\pi \alpha) + \Xi(\Omega_{\text{rf}})}{1 + \Xi(0)}. \quad (6)$$

Because of the unknown contribution of $\xi(t)$, C needs to be determined experimentally. We perform this calibration using the long-term stable axial micromotion amplitude of a single ion, as determined in PMT measurements before and afterward, as a reference (see Ref. [44]). The evaluation according to Ref. [38] yields a micromotion modulation index $\beta_i = \vec{k}_i \vec{r}_{\text{EMM}}$, where \vec{r}_{EMM} is the micromotion amplitude and \vec{k} is the laser wave vector. The rf-electric-field amplitude component along the i th laser direction can be inferred from β_i via

$$E_{\text{rf},i} = \frac{m\Omega_{\text{rf}}^2}{|\vec{k}_i|e} \beta_i = \frac{m\Omega_{\text{rf}}^2}{e} r_{i,\text{EMM}}, \quad (7)$$

where \vec{k}_i is the laser wave vector. The resulting time-dilation shift depends on E_{rf} as

$$\frac{\Delta\nu}{\nu_0} = - \left(\frac{eE_{\text{rf}}}{2mc\Omega_{\text{rf}}} \right)^2. \quad (8)$$

Conversion relations between these and other commonly used parameters to quantify EMM (such as stray-field amplitudes and equilibrium-position displacements) are summarized in the Supplemental Material [42].

C. Experimental results

Figure 4(a) shows the 3D micromotion amplitudes \vec{r}_{EMM} measured in a crystal consisting of 14 Yb^+ ions confined at $\nu_{\text{ax}} = 11.6$ kHz. In this figure, the motional amplitudes of the ions are exaggerated by a factor of 10^4 with respect to the ion distances, as the largest value is $|\vec{r}_{\text{EMM},\text{Yb}}| = 1.6$ nm. The signals are averaged over 2700 s for each of the four phases and three laser directions, and all resulting amplitude uncertainties are below 0.3 nm. The time-dilation shifts due to the mean velocities of $\vec{v}_{\text{EMM},\text{In}} = \Omega_{\text{rf}} r_{\text{EMM},\text{Yb}}/2 \cdot m_{\text{Yb}}/m_{\text{In}}$ for $^{115}\text{In}^+$ ions are shown in Fig. 4(b). Those due to axial micromotion are close to 10^{-19} for crystals up to 400 μm in length, which, depending on the axial confinement, corresponds to approximately 10 to 40 ions (at $\nu_{\text{ax}} = 10\text{--}60$ kHz). The radial components are caused by a drift of stray fields during the measurement time of more than 9 h for that crystal. As they are uniform across the crystal, more careful suppression below 10^{-19} is possible during clock operation; for example, by monitoring of the fluorescence of a single ion with a dedicated PMT during the Doppler cooling phases of the clock cycle [38]. A comparison of our method with single-ion PMT measurements, shown

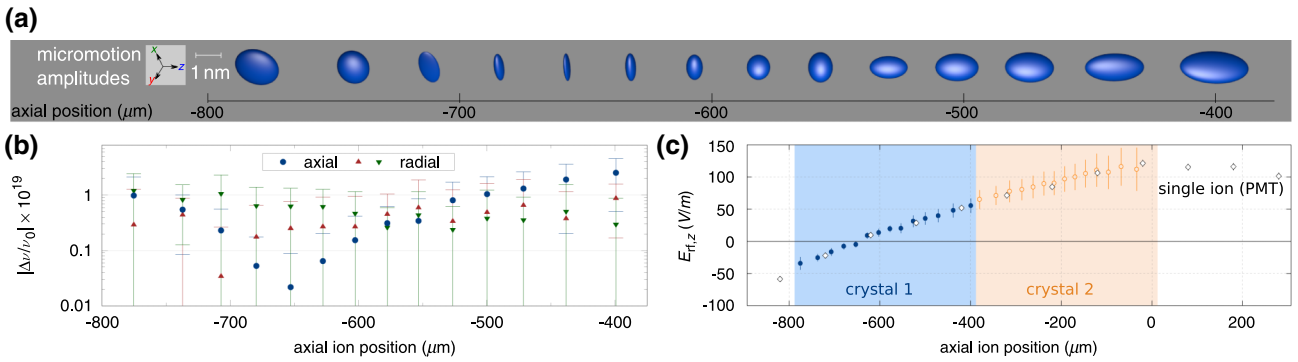


FIG. 4. Measured excess micromotion in Coulomb crystals. (a) Measured 3D micromotion amplitudes of individual ions inside a Coulomb crystal in the 2-mm segment. The small amplitudes require the use of two different length scales: ion positions refer to the black micrometer scale, while micromotion amplitudes are depicted on a nanometer scale (white bar). (b) Time-dilation shifts for $^{115}\text{In}^+$ ions due to E_{rf} at the respective positions. (c) Comparison of the axial rf fields determined in single-ion PMT measurements and by stroboscopic imaging of whole Coulomb crystals. The integration times were 2700 and 900 s per phase and direction for crystals 1 and 2, respectively. Data from the same measurement (see Supplemental Material [42] for values and uncertainties) are used in (a),(b) and in the part for crystal 1 in (c).

in Fig. 4(c) for two different crystal positions, shows matching results. This proves that in the symmetric electrode geometry chosen, the observation of a single ion is sufficient to predict the EMM amplitudes across a full linear Coulomb crystal at this level of accuracy. Further, the axial components of these measurements agree within their uncertainty over the course of more than 6 months. This means that the time-consuming micromotion measurement of the full crystal has to be performed only once to characterize the trap geometry, while fast micromotion detection of a single probe ion is sufficient during precision spectroscopy.

IV. CONCLUSION

In summary, we demonstrate an operational scalable platform for simultaneous precision spectroscopy on multiple ions with fractional frequency uncertainties at the 10^{-19} level, and show that rf-driven micromotion can be controlled in spatially extended many-body systems. Micromotion is a major uncertainty contribution in optical ion clocks and other precision measurements [45], leads to increased heating rates [36], and leads to heating and losses in ion and neutral-atom hybrid systems [46]. A full uncertainty budget for multi-ion clock operation with $^{115}\text{In}^+$, including all trap-related systematic shifts, can be found in Ref. [33]. Our findings open up the possibility to overcome the fundamental statistical uncertainty limitation of single-ion optical clocks and implement novel clock schemes (e.g., using quantum correlations in many-ion systems), while allowing systematic uncertainties at this level.

ACKNOWLEDGMENTS

We thank M. Drewsen for helpful discussions on intensifier gating electronics, N. Beev for developing the circuit,

Physikalisch-Technische Bundesanstalt departments 5.3 and 5.5 for collaboration on trap fabrication, and S.A. King for helpful comments on the manuscript. This work was supported by the DFG through Grants No. ME3648/1-1 and SFB 1227 (DQ-mat), project B03.

- [1] A. D. Ludlow, M. M. Boyd, J. Ye, E. Peik, and P. O. Schmidt, Optical atomic clocks, *Rev. Mod. Phys.* **87**, 637 (2015).
- [2] W. F. McGrew, X. Zhang, R. J. Fasano, S. A. Schäffer, K. Beloy, D. Nicolodi, R. C. Brown, N. Hinkley, G. Milani, M. Schioppa, T. H. Yoon, and A. D. Ludlow, Atomic clock performance enabling geodesy below the centimetre level, *Nature* **564**, 87 (2018).
- [3] C. Lisdat, *et al.*, A clock network for geodesy and fundamental science, *Nat. Commun.* **7**, 12443 (2016).
- [4] N. Nemitz, T. Ohkubo, M. Takamoto, I. Ushijima, M. Das, N. Ohmae, and H. Katori, Frequency ratio of Yb and Sr clocks with 5×10^{-17} uncertainty at 150 seconds averaging time, *Nat. Photonics* **10**, 258 (2016).
- [5] S. L. Campbell, R. B. Hutson, G. E. Marti, A. Goban, N. Darkwah Oppong, R. L. McNally, L. Sonderhouse, J. M. Robinson, W. Zhang, B. J. Bloom, and J. Ye, A Fermi-degenerate three-dimensional optical lattice clock, *Science* **358**, 90 (2017).
- [6] C. W. Chou, D. B. Hume, J. C. J. Koelemeij, D. J. Wineland, and T. Rosenband, Frequency Comparison of Two High-Accuracy Al^+ Optical Clocks, *Phys. Rev. Lett.* **104**, 070802 (2010).
- [7] P. Dubé, A. A. Madej, M. Tibbo, and J. E. Bernard, High-Accuracy Measurement of the Differential Scalar Polarizability of a Sr^{+88} Clock Using the Time-Dilation Effect, *Phys. Rev. Lett.* **112**, 173002 (2014).
- [8] N. Huntemann, C. Sanner, B. Lipphardt, C. Tamm, and E. Peik, Single-Ion Atomic Clock with 3×10^{-18} Systematic Uncertainty, *Phys. Rev. Lett.* **116**, 063001 (2016).

- [9] T. Pruttivarasin, M. Ramm, S. G. Porsev, I. I. Tupitsyn, M. S. Safronova, M. A. Hohensee, and H. Häffner, Michelson-Morley analogue for electrons using trapped ions to test Lorentz symmetry, *Nature* **517**, 592 (2015).
- [10] V. A. Dzuba, V. V. Flambaum, M. S. Safronova, S. G. Porsev, T. Pruttivarasin, M. A. Hohensee, and H. Häffner, Strongly enhanced effects of Lorentz symmetry violation in entangled Yb^+ ions, *Nat. Phys.* **12**, 465 (2016).
- [11] T. Rosenband, D. B. Hume, P. O. Schmidt, C. W. Chou, A. Brusch, L. Lorini, W. H. Oskay, R. E. Drullinger, T. M. Fortier, J. E. Stalnaker, S. A. Diddams, W. C. Swann, N. R. Newbury, W. M. Itano, D. J. Wineland, and J. C. Bergquist, Frequency ratio of Al^+ and Hg^+ single-ion optical clocks; metrology at the 17th decimal place, *Science* **319**, 1808 (2008).
- [12] N. Huntemann, B. Lipphardt, C. Tamm, V. Gerginov, S. Weyers, and E. Peik, Improved Limit on a Temporal Variation of m_p/m_e from Comparisons of Yb^+ and Cs Atomic Clocks, *Phys. Rev. Lett.* **113**, 210802 (2014).
- [13] R. M. Godun, P. B. R. Nisbet-Jones, J. M. Jones, S. A. King, L. A. M. Johnson, H. S. Margolis, K. Szymaniec, S. N. Lea, K. Bongs, and P. Gill, Frequency Ratio of Two Optical Clock Transitions in $^{171}\text{Yb}^+$ and Constraints on the Time Variation of Fundamental Constants, *Phys. Rev. Lett.* **113**, 210801 (2014).
- [14] A. Bjerhammar, On a relativistic geodesy, *B. Geod.* **59**, 207 (1985).
- [15] M. Vermeer, Chronometric levelling, Report of the Finnish Geodetic Institute 83, 1, 1983.
- [16] G. Lion, I. Panet, P. Wolf, C. Guerlin, S. Bize, and P. Delva, Determination of a high spatial resolution geopotential model using atomic clock comparisons, *J. Geod.* **91**, 597 (2017).
- [17] J. Müller, D. Dirx, S. M. Kopeikin, G. Lion, I. Panet, G. Petit, and P. N. A. M. Visser, High performance clocks and gravity field determination, *Space Sci. Rev.* **214**, 5 (2018).
- [18] T. E. Mehlstäubler, G. Grosche, C. Lisdat, P. O. Schmidt, and H. Denker, Atomic clocks for geodesy, *Rep. Prog. Phys.* **81**, 064401 (2018).
- [19] W. M. Itano, J. C. Bergquist, J. J. Bollinger, J. M. Gilligan, D. J. Heinzen, F. L. Moore, M. G. Raizen, and D. J. Wineland, Quantum projection noise: Population fluctuations in two-level systems, *Phys. Rev. A* **47**, 3554 (1993).
- [20] C. Champenois, M. Marcianti, J. Pedregosa-Gutierrez, M. Houssin, M. Knoop, and M. Kajita, Ion ring in a linear multipole trap for optical frequency metrology, *Phys. Rev. A* **81**, 043410 (2010).
- [21] N. Herschbach, K. Pyka, J. Keller, and T. E. Mehlstäubler, Linear Paul trap design for an optical clock with Coulomb crystals, *Appl. Phys. B* **107**, 891 (2012).
- [22] K. Arnold, E. Hajiyevev, E. Paez, C. H. Lee, M. D. Barrett, and J. Bollinger, Prospects for atomic clocks based on large ion crystals, *Phys. Rev. A* **92**, 032108 (2015).
- [23] T. Rosenband, and D. R. Leibbrandt, Exponential scaling of clock stability with atom number, arXiv:1303.6357 (2013).
- [24] J. Borregaard, and A. S. Sørensen, Efficient Atomic Clocks Operated with Several Atomic Ensembles, *Phys. Rev. Lett.* **111**, 090802 (2013).
- [25] I. D. Leroux, M. H. Schleier-Smith, and V. Vuletić, Orientation-Dependent Entanglement Lifetime in a Squeezed Atomic Clock, *Phys. Rev. Lett.* **104**, 250801 (2010).
- [26] E. M. Kessler, P. Kómár, M. Bishof, L. Jiang, A. S. Sørensen, J. Ye, and M. D. Lukin, Heisenberg-Limited Atom Clocks Based on Entangled Qubits, *Phys. Rev. Lett.* **112**, 190403 (2014).
- [27] A. V. Lebedev, P. Treutlein, and G. Blatter, Sequential quantum-enhanced measurement with an atomic ensemble, *Phys. Rev. A* **89**, 012118 (2014).
- [28] C. Schneider, D. Porras, and T. Schaetz, Experimental quantum simulations of many-body physics with trapped ions, *Rep. Prog. Phys.* **75**, 024401 (2012).
- [29] R. Blatt, and C. F. Roos, Quantum simulations with trapped ions, *Nat. Phys.* **8**, 277 (2012).
- [30] P. W. Hess, P. Becker, H. B. Kaplan, A. Kypriandis, A. C. Lee, B. Neyenhuis, G. Pagano, P. Richerme, C. Senko, J. Smith, W. L. Tan, J. Zhang, and C. Monroe, Non-thermalization in trapped atomic ion spin chains, *Phil. Trans. R. Soc. A* **375**, 20170107 (2017).
- [31] R. Blatt, and D. J. Wineland, Entangled states of trapped atomic ions, *Nature* **453**, 1008 (2008).
- [32] J. Keller, T. Burgermeister, D. Kalincev, J. Kiethe, and T. E. Mehlstäubler, Evaluation of trap-induced systematic frequency shifts for a multi-ion optical clock at the 10^{-19} level, *J. Phys. Conf. Ser.* **723**, 012027 (2016).
- [33] J. Keller, T. Burgermeister, D. Kalincev, A. Didier, A. P. Kulosa, T. Nordmann, J. Kiethe, and T. E. Mehlstäubler, Controlling systematic frequency uncertainties at the 10^{-19} level in linear Coulomb crystals, *Phys. Rev. A* **99**, 013405 (2019).
- [34] K. Pyka, N. Herschbach, J. Keller, and T. E. Mehlstäubler, A high-precision segmented Paul trap with minimized micromotion for an optical multiple-ion clock, *Appl. Phys. B* **114**, 231 (2014).
- [35] A. A. Madej, P. Dubé, Z. Zhou, J. E. Bernard, and M. Gertsvolf, $^{88}\text{Sr}^+$ 445-THz Single-Ion Reference at the 10^{-17} Level via Control and Cancellation of Systematic Uncertainties and Its Measurement against the SI Second, *Phys. Rev. Lett.* **109**, 203002 (2012).
- [36] R. B. Blakestad, C. Ospelkaus, A. P. VanDevender, J. M. Amini, J. Britton, D. Leibfried, and D. J. Wineland, High-Fidelity Transport of Trapped-Ion Qubits through an X-Junction Trap Array, *Phys. Rev. Lett.* **102**, 153002 (2009).
- [37] T. Huber, A. Lambrecht, J. Schmidt, L. Karpa, and T. Schaetz, A far-off-resonance optical trap for a Ba^+ ion, *Nat. Commun.* **5**, 5587 (2014).
- [38] J. Keller, H. L. Partner, T. Burgermeister, and T. E. Mehlstäubler, Precise determination of micromotion for trapped-ion optical clocks, *J. Appl. Phys.* **118**, 104501 (2015).
- [39] T. F. Gloger, P. Kaufmann, D. Kaufmann, M. Tanveer Baig, T. Collath, M. Johanning, and C. Wunderlich, Ion-trajectory analysis for micromotion minimization and the measurement of small forces, *Phys. Rev. A* **92**, 043421 (2015).
- [40] Z. Meir, T. Sikorsky, R. Ben-shlomi, N. Akerman, M. Pinkas, Y. Dallal, and R. Ozeri, Experimental apparatus for overlapping a ground-state cooled ion with ultracold atoms, *J. Mod. Opt.* **65**, 387 (2017).

- [41] H. Landa, M. Drewsen, B. Reznik, and A. Retzker, Modes of oscillation in radiofrequency Paul traps, *New. J. Phys.* **14**, 093023 (2012).
- [42] See Supplemental Material at <http://link.aps.org/supplemental/10.1103/PhysRevApplied.11.011002> for an estimate of collective EMM effects, EMM conversion relations, and raw data.
- [43] D. J. Berkeland, J. D. Miller, J. C. Bergquist, W. M. Itano, and D. J. Wineland, Minimization of ion micromotion in a Paul trap, *J. Appl. Phys.* **83**, 5025 (1998).
- [44] N. Beev, J. Keller, and T. E. Mehlstäubler, An avalanche transistor-based nanosecond pulse generator with high repetition rate, *Rev. Sci. Instrum.* **88**, 126105 (2017).
- [45] R. Shaniv, N. Akerman, T. Manovitz, Y. Shapira, and R. Ozeri, Quadrupole shift cancellation using dynamic decoupling, arXiv:1808.10727 (2018).
- [46] M. Cetina, A. T. Grier, and V. Vuletić, Micromotion-Induced Limit to Atom-Ion Sympathetic Cooling in Paul Traps, *Phys. Rev. Lett.* **109**, 253201 (2012).